Predictive Optimal Pulse–jet Control for Symmetric Projectiles

Bradley T. Burchett*

Rose-Hulman Institute of Technology, Terre Haute, IN, 47803

The linear theory model of a symmetric projectile is well suited to optimal control. Two methods leveraging a model predictive strategy based on closed–form trajectory solutions including relevant derivatives are developed and compared. These controllers are easily implemented using a discrete actuator such as a pulse–jet. Each controller is tested on a full six degree–of–freedom non–linear simulation, and some control parameters are tuned through appropriate trade studies.

Nomenclature

L, M, N	total external applied moment on the projectile about the mass center (ft-lb)
C_{NA}	normal force aerodynamic coefficient
C_{X0}	axial force aerodynamic coefficient
C_{LP}	roll rate damping moment aerodynamic coefficient
C_{LDD}	fin rolling moment aerodynamic coefficient
C_{MA}	pitch moment due to AOA aerodynamic coefficient
C_{MQ}	pitch rate damping moment aerodynamic coefficient
D	projectile characteristic length (ft)
$\mathbf{I}$	identity matrix
I_{xx}, I_{yy}	roll and pitch inertia expressed in the projectile reference frame (sl-ft^2)
m	projectile mass (sl)
p, q, r	angular velocity vector components expressed in the fixed plane reference frame (rad/s)
$\mathbf{R}$	optimal control weighting matrix
SL_{cg}	stationline of the projectile c.g. location (ft)
SL_{cp}	stationline of the projectile c.p. location (ft)
u, v, w	translation velocity components of the projectile center of mass resolved in the fixed plane reference frame (ft/s)
V	magnitude of the mass center velocity (ft/s)
X, Y, Z	total external applied force on the projectile expressed in the body reference frame (lb)
x, y, z	position vector components of the projectile mass center expressed in the inertial reference frame (ft)
Greek	
$\mathbf{\Phi}$	position state vector dynamics matrix
$\mathbf{\Gamma}$	position states forcing function
χ	velocity states initial condition vector
Δ_1	factor in position states forced solution
η	linear model velocity state vector $\{ \ v \quad w \quad q \quad r \ \}^T$
$\mathbf{\Psi}$	combination matrix
Λ	combination variable in the roll rate solution
ρ	air density (sl/ft^3)
ψ, θ, ϕ	Euler yaw, pitch, and roll angles (rad)
ϑ	vector of initial angular rates

*Associate Professor, Department of Mechanical Engineering, burchett@rose-hulman.edu, Associate Fellow, AIAA

Ξ	velocity state vector dynamics matrix
ξ	linear model position state vector $\{ \; y \quad z \quad \theta \quad \psi \; \}^T$

Subscript

0	Initial condition or previous state
i, j	row i, column j of matrix
p	Particular solution
t	target

I. Introduction

THROUGH several assumptions including change of independent variable from time to downrange distance travelled, projectile linear theory renders an accurate linear time–varying model of symmetric projectile flight. This model may be cast as a set of nine coupled first order ODEs and two scalar first order ODEs. Assuming the range to target is known, such a linear time varying model is readily suited to optimal control—it may be described as 'continuous with no terminal constraint, fixed terminal time (range)'.[1]

Many authors have investigated control of such projectiles, especially through model predictive schemes.[2,3,5,6] Ollerenshaw and Costello propose an optimal scheme based on discretizing the predicted and desired trajectories.[3] Schwarzmann investigated application of the LQR method to pulse–jet control of a projectile in gliding flight.[4] Both of these optimal schemes require a reference trajectory.

This work eliminates the need for a reference trajectory by predicting the impact point and its sensitivity to control correction. It also improves upon previous efforts by eliminating the need to predict the corrected trajectory.[2] A previous work[7] not only provided accurate predictions of projectile state, but also analytic derivatives of the state with respect to initial angular rates at any distance along the trajectory. Using this fast, compact trajectory predictor, and assuming the control is directly mapped to the vector of initial pitch and yaw rates, and angle of attack and sideslip velocity components, the optimal control problem may be cast as 'single stage'.[1] This leads to an optimal control scheme easily implemented using a set of pulse jets mounted near the projectile nose. Also, having predictions of both the target plane position state, and derivatives with respect to the control, an ad hoc control based on first order Taylor series approximation is proposed. The two control schemes are compared on a six degree–of–freedom simulation where a fixed number of finite discrete pulses are available.

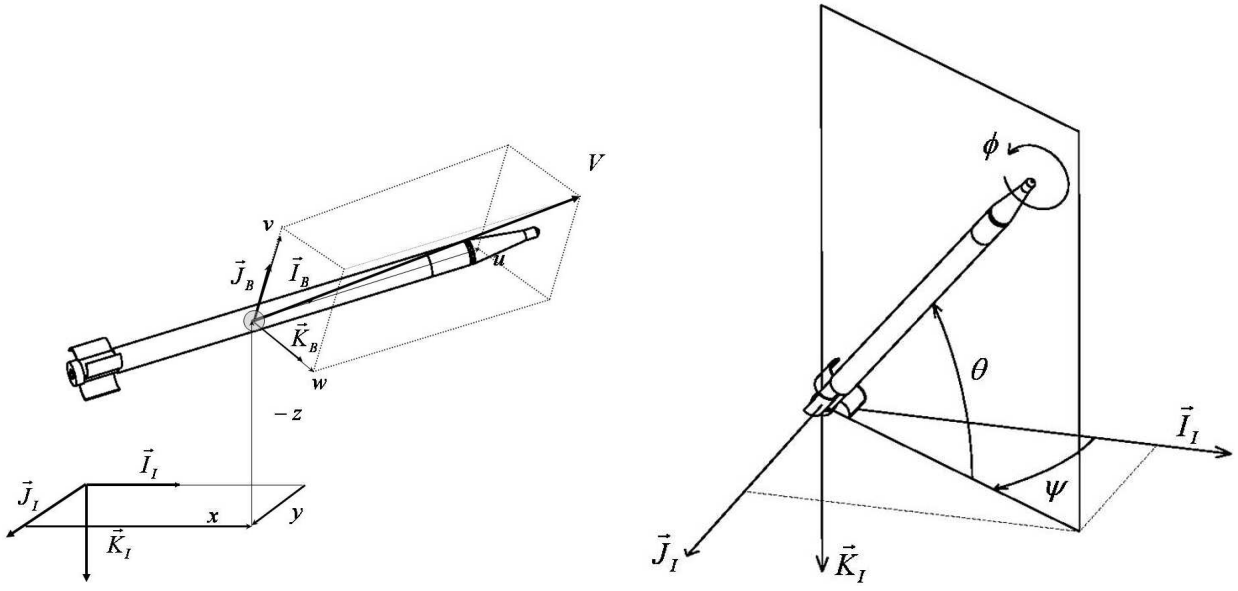

(a) Position Coordinates

(b) Attitude Coordinates

Figure 1. Schematic of a Fin Stabilized Projectile

II. Projectile Dynamic Model

The nonlinear trajectory simulation used in this study is a standard six-degree-of-freedom model typically used in flight dynamic modeling of projectiles. A schematic of the projectile configuration is shown in Figure 1. The six degrees of freedom are the components of the position vector from an inertial frame to the projectile mass center and the three standard Euler orientation angles. The equations of motion are provided in Eqs. (1-4).[2]

$$\begin{Bmatrix} \dot{x} \\ \dot{y} \\ \dot{z} \end{Bmatrix} = \begin{bmatrix} c_\theta c_\psi & s_\phi s_\theta c_\psi - c_\phi s_\psi & c_\phi s_\theta c_\psi + s_\phi s_\psi \\ c_\theta s_\psi & s_\phi s_\theta s_\psi + c_\phi c_\psi & c_\phi s_\theta s_\psi - s_\phi c_\psi \\ -s_\theta & s_\phi c_\theta & c_\phi c_\theta \end{bmatrix} \begin{Bmatrix} u \\ v \\ w \end{Bmatrix} \tag{1}$$

$$\begin{Bmatrix} \dot{\phi} \\ \dot{\theta} \\ \dot{\psi} \end{Bmatrix} = \begin{bmatrix} 1 & s_\phi t_\theta & c_\phi t_\theta \\ 0 & c_\phi & -s_\phi \\ 0 & s_\phi / c_\theta & c_\phi / c_\theta \end{bmatrix} \begin{Bmatrix} p \\ q \\ r \end{Bmatrix} \tag{2}$$

$$\begin{Bmatrix} \dot{u} \\ \dot{v} \\ \dot{w} \end{Bmatrix} = \begin{Bmatrix} X/m \\ Y/m \\ Z/m \end{Bmatrix} - \begin{bmatrix} 0 & -r & q \\ r & 0 & -p \\ -q & p & 0 \end{bmatrix} \begin{Bmatrix} u \\ v \\ w \end{Bmatrix} \tag{3}$$

$$\begin{Bmatrix} \dot{p} \\ \dot{q} \\ \dot{r} \end{Bmatrix} = [I]^{-1} \left[\begin{Bmatrix} L \\ M \\ N \end{Bmatrix} - \begin{bmatrix} 0 & -r & q \\ r & 0 & -p \\ -q & p & 0 \end{bmatrix} [I] \begin{Bmatrix} p \\ q \\ r \end{Bmatrix} \right] \tag{4}$$

In Eqs. (1) and (2), the standard shorthand notation for trigonometric functions is used: $\sin(\alpha) \equiv s_\alpha$, $\cos(\alpha) \equiv c_\alpha$, and $\tan(\alpha) \equiv t_\alpha$. The force appearing in Eq. (3) contains contributions from weight W, body aerodynamics A, and lateral pulse jets J:

$$\begin{Bmatrix} X \\ Y \\ Z \end{Bmatrix} = \begin{Bmatrix} X_W \\ Y_W \\ Z_W \end{Bmatrix} + \begin{Bmatrix} X_A \\ Y_A \\ Z_A \end{Bmatrix} + \begin{Bmatrix} X_J \\ Y_J \\ Z_J \end{Bmatrix} \tag{5}$$

Gliding flight is assumed in this study. The dynamic equations are expressed in a body-fixed reference frame, thus, all forces acting on the body are expressed in the projectile reference frame. The projectile weight force is shown in Eq. (6):

$$\begin{Bmatrix} X_W \\ Y_W \\ Z_W \end{Bmatrix} = mg \begin{Bmatrix} -s_\theta \\ s_\phi c_\theta \\ c_\phi c_\theta \end{Bmatrix} \tag{6}$$

whereas the aerodynamic force acting at the center of pressure of the projectile is given by Eq. (7):

$$\begin{Bmatrix} X_A \\ Y_A \\ Z_A \end{Bmatrix} = -\frac{\pi}{8} \rho V^2 D^2 \begin{Bmatrix} C_{X0} + C_{X2}(v^2 + w^2)/V^2 \\ C_{NA} v/V \\ C_{NA} w/V \end{Bmatrix} \tag{7}$$

The lateral pulse jets are uniformly distributed around a ring near the projectile nose. Each provides a thrust of short duration in the body $y - z$ plane such that the pulse jet force may be written as:

$$\begin{Bmatrix} X_J \\ Y_J \\ Z_J \end{Bmatrix} = \sum_{i=1}^{n_j} T_{Ji} \begin{Bmatrix} 0 \\ -\cos[2\pi(i-1)/n_j] \\ -\sin[2\pi(i-1)/n_j] \end{Bmatrix} \tag{8}$$

The applied moments about the projectile mass center contain contributions from steady aerodynamics (SA), and unsteady aerodynamics (UA).

$$\begin{Bmatrix} L \\ M \\ N \end{Bmatrix} = \begin{Bmatrix} L_{SA} \\ M_{SA} \\ N_{SA} \end{Bmatrix} + \begin{Bmatrix} L_{UA} \\ M_{UA} \\ N_{UA} \end{Bmatrix} \tag{9}$$

The moment components due to steady aerodynamic forces are computed with a cross product between the distance vector from the mass center of the projectile to the location of the specific force and the force itself. The unsteady body aerodynamic moment provides a damping source for projectile angular motion and is given by Eq. (10):

$$\left\{ \begin{array}{c} L_{UA} \\ M_{UA} \\ N_{UA} \end{array} \right\} = \frac{\pi}{8}\rho V^2 D^3 \left\{ \begin{array}{c} C_{LDD} + \frac{pDC_{LP}}{2V} \\ \frac{qDC_{MQ}}{2V} \\ \frac{rDC_{MQ}}{2V} \end{array} \right\} \tag{10}$$

The center of pressure location and all aerodynamic coefficients (C_{X0}, C_{X2}, C_{NA}, C_{LDD}, C_{LP}, and C_{MQ}) depend upon local Mach number and are computed during simulation using linear interpolation.

The dynamic equations given in Eqs. (1-4) are numerically integrated forward in time using a fourth-order, fixed-step Runge-Kutta algorithm. This non–linear plant model is used for all results and trade studies that follow.

III. Projectile Linear Theory Trajectory Predictor

The traditional linear theory assumptions result in the following set of first order differential equations.

$$x' = D \tag{11}$$

$$\phi' = \frac{D}{V}p \tag{12}$$

$$\left\{ \begin{array}{c} y' \\ z' \\ \theta' \\ \psi' \end{array} \right\} = \mathbf{\Phi} \left\{ \begin{array}{c} y \\ z \\ \theta \\ \psi \end{array} \right\} + \frac{D}{V}\mathbf{I} \left\{ \begin{array}{c} v \\ w \\ q \\ r \end{array} \right\} \tag{13}$$

Where

$$\mathbf{\Phi} = \left[\begin{array}{cccc} 0 & 0 & 0 & D \\ 0 & 0 & -D & 0 \\ 0 & 0 & 0 & 0 \\ 0 & 0 & 0 & 0 \end{array} \right]$$

$$V' = -\left[\frac{\rho SD}{2m}\right] C_{X0} V \tag{14}$$

$$p' = \frac{\rho SD^3 C_{LP}}{4I_{xx}}p + \frac{\rho SD^2 V}{2I_{xx}} C_{LDD} \tag{15}$$

The matrix equation for epicyclic pitching and yawing is:

$$\left\{ \begin{array}{c} v' \\ w' \\ q' \\ r' \end{array} \right\} = \mathbf{\Xi} \left\{ \begin{array}{c} v \\ w \\ q \\ r \end{array} \right\} + \left\{ \begin{array}{c} 0 \\ G \\ 0 \\ 0 \end{array} \right\} g \tag{16}$$

Where

$$\mathbf{\Xi} = \left[\begin{array}{cccc} -\mathbf{\Xi}_1 & 0 & 0 & -D \\ 0 & -\mathbf{\Xi}_1 & D & 0 \\ \mathbf{\Xi}_2 & \mathbf{\Xi}_3 & \mathbf{\Xi}_4 & -\mathbf{\Xi}_5 \\ -\mathbf{\Xi}_3 & \mathbf{\Xi}_2 & \mathbf{\Xi}_5 & \mathbf{\Xi}_4 \end{array} \right] \tag{17}$$

And

$$\mathbf{\Xi}_1 = \frac{\rho SD}{2m} C_{NA} \tag{18}$$

$$\Xi_3 = \frac{\rho SD}{2I_{yy}} C_{MA} \tag{19}$$

$$\Xi_4 = \frac{\rho SD^3}{4I_{yy}} C_{MQ} \tag{20}$$

$$\Xi_5 = \frac{D}{V_0} \frac{I_{xx} p}{I_{yy}} \tag{21}$$

$$G = \frac{D}{V_0} \tag{22}$$

$$C_{MA} = (SL_{COP} - SL_{CG}) C_{NA} \tag{23}$$

Ξ_2 is the Magnus term

$$\Xi_2 = \frac{\rho S}{2m} \frac{mD}{I_{yy}} \frac{D}{V} (SL_{cm} - SL_{cg}) C_{NPA} p$$

and D is the projectile characteristic length (or diameter).

III.A. Linear Predictor Closed–Form Solution

Eqs. (12–16) can be solved closed–form as follows. Eqs. (14) and (15) are decoupled from all others, resulting in the total velocity solution of

$$V(s) = V_0 \exp\left(-\frac{\rho SD}{2m} C_{X0} s \right),$$

and the roll rate solution of

$$p(s) = p_0 \Lambda + \frac{2V_0 C_{LDD}}{DC_{LP}} \exp\left(-\frac{\rho SDC_{X0}}{2m} s \right) (\Lambda - 1) \tag{24}$$

where

$$\Lambda = \exp\left(\frac{\rho SD^3 C_{LP}}{4I_{xx}} s \right). \tag{25}$$

Roll rate and total velocity are treated as time varying parameters in the remaining equations. The solution to Eq. (16) is the sum of a particular solution due to the gravity constant, and a homogeneous solution.[8] The particular solution is given by setting the derivatives equal to zero and solving the resulting algebraic equation:

$$\begin{Bmatrix} v_p \\ w_p \\ q_p \\ r_p \end{Bmatrix} = -\Xi^{-1} \begin{Bmatrix} 0 \\ G \\ 0 \\ 0 \end{Bmatrix} g \tag{26}$$

Resulting in:

$$\begin{Bmatrix} v_p \\ w_p \\ q_p \\ r_p \end{Bmatrix} = \frac{Gg}{\det(\Xi)} \begin{Bmatrix} -\Xi_5 D\Xi_3 + D\Xi_2\Xi_4 \\ D\Xi_5\Xi_3 + \Xi_1\Xi_5^2 + \Xi_1\Xi_4^2 + D\Xi_2\Xi_5 \\ -(\Xi_3\Xi_1\Xi_4 + D\Xi_3^2 + \Xi_2\Xi_1\Xi_5 + D\Xi_2^2) \\ (\Xi_3\Xi_5 - \Xi_2\Xi_4)\Xi_1 \end{Bmatrix} \tag{27}$$

Where:

$$\det(\Xi) = \Xi_1^2\Xi_5^2 + \Xi_1^2\Xi_4^2 + 2\Xi_1\Xi_1 D\Xi_3 + (D\Xi_3)^2 + 2D\Xi_2\Xi_1\Xi_5 + (D\Xi_2)^2 \tag{28}$$

This particular solution is then subtracted from the initial conditions prior to solving for the homogeneous response:

$$\chi = \eta_0 - \eta_p \tag{29}$$

The homogeneous response for epicyclic pitching and yawing may be found using the matrix exponential. The total solution is simply the sum of homogeneous and particular solutions.

$$\eta = e^{\Xi s} \chi + \eta_p \tag{30}$$

where the epicyclic velocity states are gathered into the vector $\eta = \{v,\, w,\, q,\, r\}^T$.

For the crossrange, altitude, pitch, and yaw state vector, $\xi = \{y, z, \theta, \psi\}^T$, the particular solution cannot be found by matrix inversion since $\mathbf{\Phi}$ is clearly singular. Also, the epicyclic pitching and yawing states (v, w, q, r) serve as a time varying forcing function for y, z, θ, and ψ. Thus, a general solution to forced linear systems attributed to Athans et al.[13] is invoked. For the linear system

$$\xi'(s) = \mathbf{\Phi}\xi(s) + \mathbf{\Gamma}(s) \tag{31}$$

The total solution is given as

$$\xi(s) = e^{\mathbf{\Phi}s}\xi_0 + e^{\mathbf{\Phi}s}\int_0^s e^{-\mathbf{\Phi}\tau}\mathbf{\Gamma}(\tau)d\tau \tag{32}$$

The integration is handled well by a method from Van Loan.[14,15] In the most compact form, suppose

$$\mathbf{\Psi} = \begin{bmatrix} \mathbf{\Phi} & \mathbf{\Gamma} \\ \mathbf{0} & P \end{bmatrix}. \tag{33}$$

Then

$$e^{\mathbf{\Psi}s} = \begin{bmatrix} \Omega_1 & \Delta_1 \\ \mathbf{0} & \Omega_2 \end{bmatrix} \tag{34}$$

and

$$\Omega_1 = e^{\mathbf{\Phi}s} \tag{35}$$

$$\Delta_1 = \Omega_1\int_0^s e^{-\mathbf{\Phi}\tau}\mathbf{\Gamma}e^{P\tau}d\tau. \tag{36}$$

Thus setting $P = 0$ and

$$\mathbf{\Gamma} = \frac{D}{V}\eta$$

evolution of the position state vector is computed by

$$\xi = \Omega_1\xi_0 + \Delta_1. \tag{37}$$

Note that in Eq. (33), $\mathbf{\Gamma}$ is a constant. Thus Eq. (37) is used recursively, treating η as a constant each time and averaging it with the previous velocity state for improved accuracy. Practically, $\mathbf{\Gamma}$ is computed simply by

$$\mathbf{\Gamma} = \frac{D}{2V}(\eta + \eta_0)$$

in the actual algorithm.

III.B. Linear Predictor Closed–Form Derivatives

Analytic derivatives of the position state vector ξ wrt an initial angular rate ϑ_i may then be found by differentiating Eq. (37) resulting in

$$\frac{\partial\xi}{\partial\vartheta_i} = \Omega_1\frac{\partial\xi_0}{\partial\vartheta_i} + \frac{\partial\Delta_1}{\partial\vartheta_i}. \tag{38}$$

Since Ω_1 is a constant, the potential term involving derivatives of Ω_1 does not appear. Thus in addition to previous calculations, only the forced part of the position state vector solution needs to be differentiated

$$\frac{\partial\Delta_1}{\partial\vartheta_i} = \int_0^s e^{-\mathbf{\Phi}\tau}\frac{\partial\mathbf{\Gamma}}{\partial\vartheta_i}d\tau \tag{39}$$

which can be found from once again invoking the Van Loan formula with

$$\frac{\partial}{\partial\vartheta_i}\mathbf{\Psi} = \begin{bmatrix} \mathbf{\Phi} & \frac{\partial}{\partial\vartheta_i}\mathbf{\Gamma} \\ \mathbf{0} & 0 \end{bmatrix} \tag{40}$$

Such that

$$\exp\left(s\frac{\partial}{\partial\vartheta_i}\mathbf{\Psi}\right) = \begin{bmatrix} \Omega_3 & \frac{\partial\Delta_1}{\partial\vartheta_i} \\ 0 & \Omega_4 \end{bmatrix} \tag{41}$$

And $\partial\mathbf{\Gamma}/\partial\vartheta_i$ is found from differentiating the closed form solution for the velocity state vector $\eta = \{v\ w\ q\ r\ \}^T$.

Initial sideslip, angle of attack, pitch and yaw rates influence the initial values of the η vector as

$$\begin{aligned}
\left.\frac{\partial\eta}{\partial v_0}\right|_{s=0} &= e^{\mathbf{\Xi}}\left\{\begin{array}{cccc} 1 & 0 & 0 & 0 \end{array}\right\}^T \\
\left.\frac{\partial\eta}{\partial w_0}\right|_{s=0} &= e^{\mathbf{\Xi}}\left\{\begin{array}{cccc} 0 & 1 & 0 & 0 \end{array}\right\}^T \\
\left.\frac{\partial\eta}{\partial q_0}\right|_{s=0} &= e^{\mathbf{\Xi}}\left\{\begin{array}{cccc} 0 & 0 & 1 & 0 \end{array}\right\}^T \\
\left.\frac{\partial\eta}{\partial r_0}\right|_{s=0} &= e^{\mathbf{\Xi}}\left\{\begin{array}{cccc} 0 & 0 & 0 & 1 \end{array}\right\}^T
\end{aligned}$$

This influence must then be propagated along the trajectory, therefore $\partial\eta/\partial v_0$, $\partial\eta/\partial w_0$, $\partial\eta/\partial q_0$, and $\partial\eta/\partial r_0$ are treated as co–states which are updated by

$$\begin{aligned}
\left.\frac{\partial\eta}{\partial v_0}\right|_{s=k} &= e^{\mathbf{\Xi}}\left.\frac{\partial\eta}{\partial v_0}\right|_{s=k-1} \\
\left.\frac{\partial\eta}{\partial w_0}\right|_{s=k} &= e^{\mathbf{\Xi}}\left.\frac{\partial\eta}{\partial w_0}\right|_{s=k-1} \\
\left.\frac{\partial\eta}{\partial q_0}\right|_{s=k} &= e^{\mathbf{\Xi}}\left.\frac{\partial\eta}{\partial q_0}\right|_{s=k-1} \\
\left.\frac{\partial\eta}{\partial r_0}\right|_{s=k} &= e^{\mathbf{\Xi}}\left.\frac{\partial\eta}{\partial r_0}\right|_{s=k-1}
\end{aligned}$$

Derivatives of the position states wrt v_0, w_0, q_0 and r_0 are then computed by respective instances of Eq. 38 where

$$\begin{aligned}
\frac{\partial\mathbf{\Gamma}}{\partial v_0} &= \frac{D}{V_0}\left.\frac{\partial\eta}{\partial v_0}\right|_{s=k} \\
\frac{\partial\mathbf{\Gamma}}{\partial w_0} &= \frac{D}{V_0}\left.\frac{\partial\eta}{\partial w_0}\right|_{s=k} \\
\frac{\partial\mathbf{\Gamma}}{\partial q_0} &= \frac{D}{V_0}\left.\frac{\partial\eta}{\partial q_0}\right|_{s=k} \\
\frac{\partial\mathbf{\Gamma}}{\partial r_0} &= \frac{D}{V_0}\left.\frac{\partial\eta}{\partial r_0}\right|_{s=k}
\end{aligned}$$

Practical calculation of Ω_1, Δ_1, and their derivatives are discussed in the sequel.

III.C. Some Notes on Practical Computation

The matrix exponential of Eqs. (34) and (41) will need to be evaluated once for each trajectory prediction step, and once for each step of each of the derivative predictions respectively. In order to reduce computational burden, use of the series expansion

$$e^{\mathbf{\Psi}s} = \mathbf{I} + \mathbf{\Psi}s + \frac{1}{2!}\mathbf{\Psi}^2s^2 + \frac{1}{3!}\mathbf{\Psi}^3s^3 + \cdots$$

is explored and due to the sparsity of $\mathbf{\Psi}$, $\mathbf{\Psi}^n = 0\,\forall\, n \geq 3$. Thus the series expansion for $e^{\mathbf{\Psi}s}$ converges in just three terms, that is:

$$e^{\mathbf{\Psi}s} = \mathbf{I} + \mathbf{\Psi}s + \frac{1}{2!}\mathbf{\Psi}^2s^2.$$

Since $\mathbf{\Phi}$ is invariant with respect to aerodynamic parameters, $\mathbf{\Psi}$ is partitioned into variant and invariant parts in hopes of speeding up computation of the derivatives of Δ_1. This results in

$$e^{\mathbf{\Psi}s} = \begin{bmatrix} \mathbf{I} & 0 \\ 0 & 1 \end{bmatrix} + \begin{bmatrix} \mathbf{\Phi} & \mathbf{\Gamma} \\ 0 & 0 \end{bmatrix} s + \frac{1}{2!} \begin{bmatrix} \mathbf{\Phi}^2 & \mathbf{\Phi\Gamma} \\ 0 & 0 \end{bmatrix} s^2$$

and since $\mathbf{\Phi}^2 = 0$, Ω_1 and Δ_1 are computed directly by

$$\Omega_1 = \mathbf{I} + \mathbf{\Phi}s \tag{42}$$

$$\Delta_1 = \mathbf{\Gamma}s + \frac{1}{2!}\mathbf{\Phi\Gamma}s^2 \tag{43}$$

Thus derivatives, of the position states are found simply by evaluating Eq. (44).

$$\frac{\partial \Delta_1}{\partial \vartheta_i} = \frac{\partial \Gamma}{\partial \vartheta_i}s + \frac{1}{2!}\mathbf{\Phi}\frac{\partial \Gamma}{\partial \vartheta_i}s^2 \tag{44}$$

The linear theory solutions are solved recursively such that $\{v_0,\, w_0,\, q_0,\, r_0\}$ represents the solution at the last sample and $\{v,\, w,\, q,\, r\}$ and $\{v_p,\, w_p,\, q_p,\, r_p\}$ are the respective quantities at the current sample.

IV. Predictive Control Strategies

IV.A. Taylor Series Controller

Since both the target plane position states and their derivatives with respect to angular rates are available from solution of the linear theory model, a brute force control scheme may be found by writing the impact point state as a first order Taylor series.

$$\begin{Bmatrix} y_t \\ z_t \\ \theta_t \\ \psi_t \end{Bmatrix} = \begin{Bmatrix} \hat{y} \\ \hat{z} \\ \hat{\theta} \\ \hat{\psi} \end{Bmatrix} + \begin{bmatrix} \frac{\partial y}{\partial v_0} & \frac{\partial y}{\partial w_0} & \frac{\partial y}{\partial q_0} & \frac{\partial y}{\partial r_0} \\ \frac{\partial z}{\partial v_0} & \frac{\partial z}{\partial w_0} & \frac{\partial z}{\partial q_0} & \frac{\partial z}{\partial r_0} \\ \frac{\partial \theta}{\partial v_0} & \frac{\partial \theta}{\partial w_0} & \frac{\partial \theta}{\partial q_0} & \frac{\partial \theta}{\partial r_0} \\ \frac{\partial \psi}{\partial v_0} & \frac{\partial \psi}{\partial w_0} & \frac{\partial \psi}{\partial q_0} & \frac{\partial \psi}{\partial r_0} \end{bmatrix} \begin{Bmatrix} \delta v_0 \\ \delta w_0 \\ \delta q_0 \\ \delta r_0 \end{Bmatrix} \tag{45}$$

Previous studies have shown that a divert event such as a discrete pulse jet has the effect of 'resetting' the angular rates. Thus, Eq. (45) is solved for the desired angular rates resulting in Eq. (46).

$$\begin{Bmatrix} \delta v_0 \\ \delta w_0 \\ \delta q_0 \\ \delta r_0 \end{Bmatrix} = - \begin{bmatrix} \frac{\partial y}{\partial v_0} & \frac{\partial y}{\partial w_0} & \frac{\partial y}{\partial q_0} & \frac{\partial y}{\partial r_0} \\ \frac{\partial z}{\partial v_0} & \frac{\partial z}{\partial w_0} & \frac{\partial z}{\partial q_0} & \frac{\partial z}{\partial r_0} \\ \frac{\partial \theta}{\partial v_0} & \frac{\partial \theta}{\partial w_0} & \frac{\partial \theta}{\partial q_0} & \frac{\partial \theta}{\partial r_0} \\ \frac{\partial \psi}{\partial v_0} & \frac{\partial \psi}{\partial w_0} & \frac{\partial \psi}{\partial q_0} & \frac{\partial \psi}{\partial r_0} \end{bmatrix}^{-1} \begin{Bmatrix} \hat{y} - y_t \\ \hat{z} - z_t \\ \hat{\theta} - \theta_t \\ \hat{\psi} - \psi_t \end{Bmatrix} \tag{46}$$

Preliminary use of Eq. (46) to determine the control gave less than satisfactory performance. Since there are no constraints on pitch and yaw at the target, the bottom two rows are discarded.

Two replacement constraints are found by matching inertia properties with the effect of pulse jets mounted near the projectile nose. Previous work[17] offers the following relationships

$$\delta v_0 = \frac{Y_{Jnr}}{m} \tag{47}$$

$$\delta r_0 = \frac{R_{Ix} Y_{Jnr}}{I_{yy}} \tag{48}$$

$$\delta w_0 = \frac{Z_{Jnr}}{m} \tag{49}$$

$$\delta q_0 = -\frac{Z_{Jnr} R_{Ix}}{I_{yy}} \tag{50}$$

Where Y_{Jnr} and Z_{Jnr} are the y and z components respectively of an impulse applied in the no roll frame and R_{Ix} is the stationline distance from center of mass to point of impulse application. Solving Eqs. (47) and

(48) for Y_{Jnr} and equating, then solving Eqs. (49) and (50) for Z_{Jnr} and equating, the following constraints emerge.

$$\left\{ \begin{array}{c} 0 \\ 0 \end{array} \right\} = \left[\begin{array}{cccc} m & 0 & 0 & -\frac{I_{yy}}{R_{Ix}} \\ 0 & m & \frac{I_{yy}}{R_{Ix}} & 0 \end{array} \right] \left\{ \begin{array}{c} \delta v_0 \\ \delta w_0 \\ \delta q_0 \\ \delta r_0 \end{array} \right\}$$

These are used in place of the bottom two rows of the Jacobian and residual in Eq. (45). The resulting control is then found by modifying Eq. (46) in similar fashion. The divert commands must be transformed into the body frame and compared to a threshold before a pulse–jet is fired. Since these details are common to both strategies, they are discussed later.

IV.B. Single Stage Optimal Control

Given the impact point prediction and estimates of impact point sensitivity to changes of initial angular rates, evolution of the impact point due to impulse control may be modeled as a single stage system.

$$\mathbf{x}(1) = \mathbf{f}^0\left(\mathbf{x}(0), \mathbf{u}(0)\right)$$

This is a well studied problem,[1] however the application is novel. Using primarily Bryson's notation, the details are unpacked as follows. The state evolution eqn. needs only describe the change in impact point due to change in initial angular rates

$$\left\{ \begin{array}{c} y(1) \\ z(1) \end{array} \right\} = \left\{ \begin{array}{c} y(0) \\ z(0) \end{array} \right\} + \left[\begin{array}{cccc} \frac{\partial y}{\partial v_0} & \frac{\partial y}{\partial w_0} & \frac{\partial y}{\partial q_0} & \frac{\partial y}{\partial r_0} \\ \frac{\partial z}{\partial v_0} & \frac{\partial z}{\partial w_0} & \frac{\partial z}{\partial q_0} & \frac{\partial z}{\partial r_0} \end{array} \right] \left\{ \begin{array}{c} \delta v_0 \\ \delta w_0 \\ \delta q_0 \\ \delta r_0 \end{array} \right\} \tag{51}$$

or

$$\mathbf{x}(1) = \mathbf{x}(0) + \mathbf{B}\mathbf{u}(0).$$

Given the cost function

$$J = \phi(\mathbf{x}(1)) + \mathbf{u}^T(0)\mathbf{R}\mathbf{u}(0)$$

The Hamiltonian function is

$$\tilde{H} = \mathbf{u}^T(0)\mathbf{R}\mathbf{u}(0) + \lambda^T(1)\left[\mathbf{x}(0) + \mathbf{B}\mathbf{u}(0)\right]$$

Where $\mathbf{B}$ is the 2×4 Jacobian matrix. The Euler–Lagrange equations are

$$\frac{\partial \tilde{H}}{\partial \mathbf{u}(0)} = 0 \rightarrow 0 = \mathbf{u}^T\mathbf{R} + \lambda^T\mathbf{B}$$

or

$$\mathbf{R}\mathbf{u} + \mathbf{B}^T\lambda = 0$$

and

$$\lambda^T(1) = \frac{\partial \phi}{\partial \mathbf{x}(1)}$$

By choosing $\mathbf{R} > 0$, and $\phi(\mathbf{x}(1)) = \mathbf{x}^T(1)\mathbf{x}(1)/2$, the control is found to be

$$\mathbf{u} = -\mathbf{R}^{-1}\mathbf{B}^T\lambda \tag{52}$$

and the co–states are

$$\lambda = \left\{ \begin{array}{c} y(1) \\ z(1) \end{array} \right\}. \tag{53}$$

If the magnitude of all controls are limited equally by choosing $\mathbf{R} = \gamma\mathbf{I}$ where γ is a positive scalar, then the optimal control is

$$\left\{ \begin{array}{c} \delta v_0 \\ \delta w_0 \\ \delta q_0 \\ \delta r_0 \end{array} \right\} = -\frac{1}{\gamma} \left[\begin{array}{cc} \frac{\partial y}{\partial v_0} & \frac{\partial z}{\partial v_0} \\ \frac{\partial y}{\partial w_0} & \frac{\partial z}{\partial w_0} \\ \frac{\partial y}{\partial q_0} & \frac{\partial z}{\partial q_0} \\ \frac{\partial y}{\partial r_0} & \frac{\partial z}{\partial r_0} \end{array} \right] \left\{ \begin{array}{c} y(1) \\ z(1) \end{array} \right\} \tag{54}$$

Unlike the previous method, a matrix inverse is not required, and the controls need not be constrained with respect to inertia properties.

IV.C. Pulse–jet Control Allocation

Both control schemes yield a vector of commanded angular rate perturbations in the no roll frame. In order to implement the command via a finite magnitude pulse–jet mounted to the rocket body, the perturbation must first be transformed to the body frame. This is done by first determining $\{\delta v_0,\, \delta w_0,\, \delta q_0,\, \delta r_0\}^T$ then using Eqs. (47) and (49) to solve for Y_{Jnr}, Z_{Jnr}. The roll angle at which a pulse jet is required is then found by relating the no–roll frame pulse components Y_{Jnr}, Z_{Jnr} with the roll frame pulse components Y_J, Z_J shown in Eq. 8. These formulas can be rearranged as

$$\begin{bmatrix} -Y_J(i) & -Z_J(i) \\ Z_J(i) & -Y_J(i) \end{bmatrix} \begin{Bmatrix} \cos(\phi) \\ \sin(\phi) \end{Bmatrix} = \begin{Bmatrix} Y_{Jnr} \\ Z_{Jnr} \end{Bmatrix} \tag{55}$$

which are inverted to isolate $\cos(\phi)$ and $\sin(\phi)$

$$\begin{Bmatrix} \cos(\phi) \\ \sin(\phi) \end{Bmatrix} = \frac{1}{Y_J(i)^2 + Z_J(i)^2} \begin{bmatrix} -Y_J(i) & Z_J(i) \\ -Z_J(i) & -Y_J(i) \end{bmatrix} \begin{Bmatrix} Y_{Jnr} \\ Z_{Jnr} \end{Bmatrix} \tag{56}$$

such that:

$$\cos\phi = \left(-Y_J(i)Y_{Jnr} + Z_J(i)Z_{Jnr}\right) / \left(Y_J(i)^2 + Z_J(i)^2\right) \tag{57}$$

$$\sin\phi = \left(-Z_J(i)Y_{Jnr} - Y_J(i)Z_{Jnr}\right) / \left(Y_J(i)^2 + Z_J(i)^2\right) \tag{58}$$

Finally, the four-quadrant arc tangent is invoked to find $\phi = \texttt{atan2}(\sin(\phi), \cos(\phi))$. From this desired angle and the current roll rate, a time to fire the next unused pulse jet i is estimated.

Second, the magnitude of the commanded perturbation will never match the control authority of a single pulse. Thus the desired pulse magnitude, $\sqrt{Y_{Jnr}^2 + Z_{Jnr}^2}$, is compared to a threshold. If the magnitude exceeds this threshold, the pulse jet is fired; if not, the projectile continues downrange without correction, as the perturbation required to move the impact point a fixed distance increases as the distance to target plane decreases. Note that the specific threshold value must be chosen to allow some overshoot, otherwise the pulse–jet would only be fired in situations resulting in undershoot. The final threshold value for each control scheme is chosen through a trade study.

V. Results

The control strategies were tested on the non–linear plant model shown in Section II. Projecile parameters were chosen similar to the 'Hydra 70' 2.75 inch diameter rocket. The target is defined as (7582.0,0,0) ft in the gun tube fixed right handed (x, y, z) frame where x points downrange, y to the right, and z points down. Initial conditions were determined from a six DOF non-linear simulation of the powered phase of flight. At motor cut–off the rocket mass center was at the origin with $\phi = 0$ rad, $\psi = 0$ rad, v=0 ft/s, w=0 ft/s, p=-58.928 rad/s, q=0 rad/s, r=-0.039385 rad/s, and V=2177.7 ft/s.

The initial pitch and yaw angles (θ, ψ) were assumed to vary according to independent uniform distributions with means of 0.0348 and 0.00122 and variances of $3.11(10)^{-5}$ and $3.88(10)^{-5}$ rad respectively. This Monte Carlo set was tested first with no control, resulting in the dispersion shown in Figure

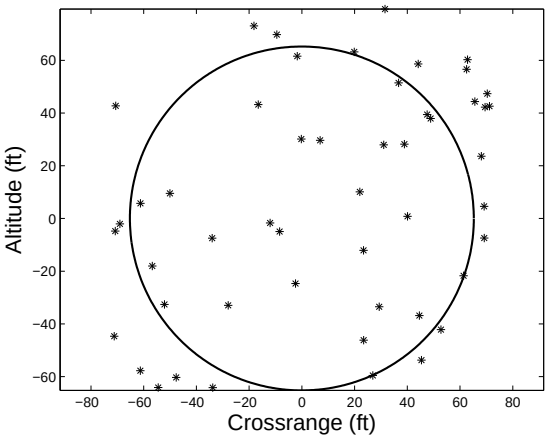

Figure 2. Monte Carlo Results - Uncontrolled Dispersion

2. The uncontrolled dispersion has a circular error probable (CEP, i.e. the median miss distance) of 65.228 ft.

The control schemes were tested assuming a pulse jet array of 12 pulses each with an impulse of 1.12 lb–s. The six DOF simulation assumes that each pulse exerts a constant thrust over a 5 ms period. The control logic in both cases has two adjustable parameters which are a correction threshold, and the time between subsequent trajectory predictions. The latter parameter limits the computational effort and provides time for the projectile to settle after a pulse is fired. The threshold attempts to postpone pulse firing until overshoot is minimal. Early corrections result in greater swerve at the target plane, thus by setting a correction threshold small corrections will be achieved by pulsing further downrange. If both parameters have ideal values, the

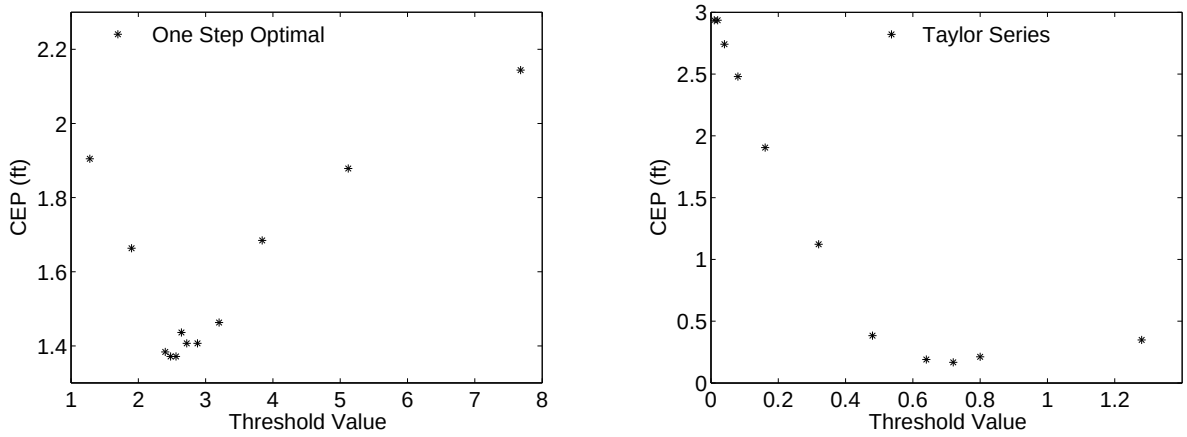

(a) One Step Optimal

(b) Taylor Series

Figure 3. Tuning the Threshold Parameter

predictions would happen frequently enough, and the threshold would be tuned such that the last correction would move the impact point to the target. Since the pulse has a discrete, immutable size, and is only properly aligned once per roll cycle, some dispersion will always remain. Also, there is little or no benefit to predicting the trajectory more than once per roll cycle.

The time between trajectory predictions was set at 0.1 sec, slightly less than one roll cycle. This provides a good balance between computational effort (simulation time) and accuracy. Each of the control schemes was then tuned for minimum median miss distance (CEP) by adjusting the correction threshold as shown in Figure 3. The best performance observed using the Taylor series controller was a CEP of 0.167 ft using a threshold of 0.72. The corresponding dispersion is shown in Figure 4a. The best performance of the one step optimal controller resulted in a CEP of 1.37 ft using a threshold of 2.48 as shown in Fig. 4b.

Note the difference in axis scaling between Figures 4a and b. This indicates that the Taylor series has an average miss distance approximately one order of magnitude smaller than that for one step optimal. Also note the size of the CEP circle in Fig. 4b compared to the frame size. The CEP circle appears much smaller in Fig. 4b, indicating that the distribution of impacts for one–step optimal is more widely spread than that of the Taylor series, i.e. outliers miss by a larger proportion of CEP.

Overall, the Taylor Series controller performs significantly better, most likely due to the extra information in the matrix inversion which 'coordinates' the pulse with projectile inertia properties. Performance of the controllers is similar due to the limited information (direction) used in control allocation and the finite, discrete nature of each correction.

VI. Conclusions

Two candidate optimal control strategies were derived from a linear model of symmetric projectile flight and its closed–form solution. Performance was demonstrated on a non–linear 6DOF simulation. The Taylor Series Controller, using a full Jacobian matrix inversion to calculate desired pulse magnitude and direction, performed significantly better than the one step optimal controller as measured by CEP. Furthermore, impact

points outisde of the CEP circle were scattered proportionally wider using the one–step optimal controller. Performance of both controllers was hindered by the inability to dynamically adjust the magnitude and number of pulses.

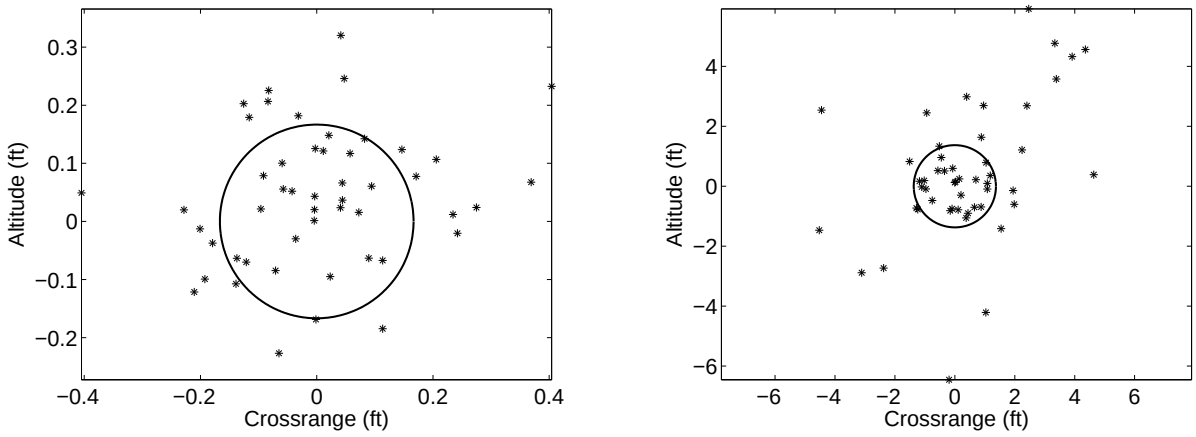

(a) Taylor Series

(b) One Step Optimal

Figure 4. Monte Carlo Results - Controlled Dispersions

References

[1]Bryson, A. E., and Ho, Y., *Applied Optimal Control*, Ginn and Company, Waltham, MA, 1969.

[2]Burchett, B. T., and Costello, M., "Model Predictive Lateral Pulse Jet Control of an Atmospheric projectile," *Journal of Guidance, Control, and Dynamics*, Vol 25, No. 5, pp. 860-867, September-October 2002.

[3]Ollerenshaw, D., and Costello, M., "Model Predictive Control of a Direct Fire Projectile Equipped with Canards," 2005 AIAA Atmospheric Flight Mechanics Conference, San Francisco, California, 15–18 August, 2005.

[4]Schwarzmann, D., *Optimal Jet Thruster Control of an Atmospheric Rocket*, M.S. Thesis, Rose–Hulman Institute of Technology, 2003.

[5]Slegers, N. "Predictive Control of a Munition Using Low–Speed Linear Theory," *Journal of Guidance, Control, and Dynamics*, Vol 31, No. 3, pp. 768–775, May–June 2008.

[6]Fresconi, F., and Ilg, M., "Model Predictive Control of Agile Projectiles" 2012 AIAA Atmospheric Flight Mechanics Conference, Minneapolis, Minnesota, 13–16 August, 2012, AIAA 2012–4860.

[7]Burchett, B. T., "Aerodynamic Parameter Identification for Symmetric Projectiles: An Improved Gradient Based Method", AIAA Atmospheric Flight Mechanics Conference, Minneapolis, Minnesota, 13–16 August, 2012, AIAA 2012–4861.

[8]Burchett, B., Peterson, A., and Costello, M., "Prediction of Swerving Motion of a Dual-Spin Projectile with Lateral Pulse Jets in Atmospheric Flight," *Mathematical and Computer Modelling*, Vol. 35, pp. 821-834, 2002.

[9]Kwakernaak, H., and Sivan, R., *Linear Optimal Control Systems*, Wiley, New York, 1972.

[10]Guidos, B., and Cooper, G., "Linearized Motion of a Fin-Stabilized Projectile Subjected to a Lateral Impulse," *Journal of Spacecraft and Rockets*, Vol. 39, No. 3, pp. 384-391, May 2002.

[11]Guidos, B., "Deflection Measurement Accuracy in a Course–Corrected 120–mm Mortar Spark Range Flight Experiment," 2004 AIAA Atmospheric Flight Mechanics Conference, Providence, Rhode Island, 16–19 August, 2004.

[12]Hainz, L. C. III, and Costello, M., "Modified Projectile Linear Theory for Rapid Trajectory Prediction," *Journal of Guidance, Control, and Dynamics*, Vol 28, No. 5, pp. 1006–1014, September–October 2005.

[13]Athans, M., Dertouzos, M. L., Spann, R. N., and Mason, S. J., *Systems, Networks, and Computation: Multivariable Methods*, McGraw-Hill, 1974.

[14]Van Loan, C., "Computing integrals involving the matrix exponential," *IEEE Transactions on Automatic Control*, Vol. 23, No. 3, pp. 395-404, 1978.

[15]Burchett, B., and Costello, M., "A Numerical Technique for Optimal Output Feedback Using Pade Approximations," 2001 AIAA Guidance, Navigation and Control Conference, Montreal, Quebec, Canada, Paper No. AIAA 2001-4352, 2001.

[16]Press, W. H., et al., *Numerical Recipes in Fortran, 2nd Ed.*, Cambridge, 1992.

[17]Burchett, B. T., *Robust Lateral Pulse Jet Control of an Atmospheric projectile*, Ph.D. Thesis, Oregon State University, 2001.